Quark matter with an anisotropic momentum distribution

Wei-bo He[1,2] and Guo-yun Shao[1,*]

[1]*MOE Key Laboratory for Non-equilibrium Synthesis and Modulation of Condensed Matter, School of Physics, Xi'an Jiaotong University, Xi'an 710049, China*

[2]*School of Physics, Peking University, Beijing, 100871, China*

(Received 5 July 2023; accepted 29 November 2023; published 14 December 2023)

Motivated by the anisotropic momentum distribution of particles in heavy-ion collisions, we study the angular dependence of quark average momentum and quark distribution function in the Polyakov-Nambu-Jona-Lasinio quark model. We also investigate the phase transitions and net baryon number fluctuations in anisotropic quark matter. The numerical results suggest that the QCD phase structure and isentropic trajectories are sensitive to the anisotropic parameter at finite density, in particular, in the area near the critical region and the first-order phase transition. Compared with the isotropic quark matter, the values of baryon number kurtosis and skewness at lower collision energies are possibly enhanced with the anisotropic momentum distribution squeezed along the direction of nucleus-nucleus collision in experiments.

DOI: 10.1103/PhysRevD.108.114012

I. INTRODUCTION

Exploring the phase structure of quantum chromodynamics (QCD) is an important topic in both theoretical and experimental nuclear physics. The calculation from lattice QCD indicates that the transformation from quark-gluon plasma (QGP) to hadrons is a smooth crossover [1–8] at vanishing and small baryon chemical potentials. Many QCD inspired models/approaches further predict that there exists a first-order phase transition with a critical end point (CEP) connecting with a crossover transformation at finite temperature and chemical potential (e.g., [9–23]). The QCD phase structure can be probed due to the energy-dependent behavior of the ratios of net-baryon number fluctuations at chemical freeze-out [24]. The cumulants of net proton (proxy for baryon) have been measured in the Beam Energy Scan experiments at RHIC STAR, and the nonmonotonic energy dependence of the net-proton number fluctuations have been discovered [25–27]. The experimental data has aroused a wide discussion about whether the QCD critical region has been reached.

The isotropic momentum distribution is usually assumed to explore the phase structure in lattice QCD simulations and QCD inspired models. However, deviations from perfect isotropy are expected for a real quark-gluon plasma. A large momentum-space anisotropy can arise due to the rapid longitudinal expansion of the matter created in relativistic heavy ion collisions and the anisotropy possibly survive during the entire evolution of the medium [28]. A similar result exists in hydrodynamic simulations. The ideal relativistic hydrodynamics predict that the QGP would tends to be isotropic on a timescale $\tau \sim 0.5$ fm/c [29,30]. In practice, however, with the inclusion of viscous correction sizable differences between the transverse and longitudinal pressure can still be observed at times $\tau \lesssim 2$ fm/c [31–38]. Recently, the anisotropic hydrodynamics has also been developed to account for large deviations from isotropy in momentum space, which provides a more accurate description of nonequilibrium dynamics than usual relativistic hydrodynamic models [39–43].

A natural question aroused is how the anisotropic momentum distribution affects the QCD phase transition and final observables in experiments. To answer this question, it is necessary to explore various properties of anisotropic QGP. The anisotropic distribution of particles in momentum space can be phenomenologically described by introducing a spheroidally anisotropic distribution function by stretching or squeezing the isotropic distribution along one of the directions. In Ref. [44], a popular one-particle distribution function in anisotropic momentum space was first proposed in the pioneer work by Romatschke and Strickland, $f^{\mathrm{aniso}}(\mathbf{p}) = [\exp[(\sqrt{\mathbf{p}^2 + \xi(\mathbf{p}\cdot\mathbf{n})^2 + m^2} - \mu)/T] \pm 1]^{-1}$, where ξ is a parameter indicating the strength and type of momentum-space anisotropy and $\mathbf{n}$ is the anisotropy direction. Such a parametrization is interesting in heavy-ion collisions with the parton distribution to be squeezed along the beam direction. By far, the anisotropic distribution in

*Corresponding author: gyshao@mail.xjtu.edu.cn

Published by the American Physical Society under the terms of the Creative Commons Attribution 4.0 International license. Further distribution of this work must maintain attribution to the author(s) and the published article's title, journal citation, and DOI. Funded by SCOAP[3].

momentum space has been considered to study various issues, such as, collective modes [45], quarkonium states [46,47], photon and dilepton production [48,49], as well as transport coefficients [50,51].

In this work, we focus on exploring the phase transition in anisotropic QCD medium. Since the fluctuations of conserved charges are closely related to QCD phase transitions [22,52,53] and are also the sensitive probes to diagnose the QCD phase structure in HIC experiments [24–27], we further explore the correlation of baryon number fluctuations with the phase transitions in anisotropic QCD matter. The potential impact on experimental data analysis of baryon number fluctuations are also discussed. The 2 + 1 flavor PNJL quark model is taken in the calculation, which describe well both the chiral phase transition and (de)confinement phase transition of QCD.

II. FORMULAS FOR QUARK MATTER WITH AN ANISOTROPIC MOMENTUM DISTRIBUTION

We first simply introduce the thermodynamic formulas for isotropic quark matter, and then extend the relevant formulas to the case of anisotropy in momentum space. The Lagrangian density in the 2 + 1 flavor PNJL model is given by [22,54]

$$\begin{aligned}\mathcal{L} &= \bar{q}(i\gamma^\mu D_\mu + \gamma_0\hat{\mu} - \hat{m}_0)q + G\sum_{k=0}^{8}[(\bar{q}\lambda_k q)^2 + (\bar{q}i\gamma_5\lambda_k q)^2] \\ &\quad - K[\mathtt{det}_f(\bar{q}(1+\gamma_5)q) + \mathtt{det}_f(\bar{q}(1-\gamma_5)q)] \\ &\quad - U(\Phi[A], \bar{\Phi}[A], T), \end{aligned} \tag{1}$$

where q denotes the quark fields with three flavors, u, d, and s; $\hat{m}_0 = \mathtt{diag}(m_u, m_d, m_s)$ in flavor space; G and K are the four-point and six-point interacting constants, respectively. The $\hat{\mu} = \mathrm{diag}(\mu_u, \mu_d, \mu_s)$ are the quark chemical potentials.

The covariant derivative in the Lagrangian is defined as $D_\mu = \partial_\mu - iA_\mu$. The gluon background field $A_\mu = \delta^0_\mu A_0$ is supposed to be homogeneous and static, with $A_0 = g\mathcal{A}_0^\alpha \frac{\lambda^\alpha}{2}$, where $\frac{\lambda^\alpha}{2}$ is $SU(3)$ color generators. The effective potential $U(\Phi[A], \bar{\Phi}[A], T)$ is expressed with the traced Polyakov loop $\Phi = (\mathrm{Tr}_c L)/N_C$ and its conjugate $\bar{\Phi} = (\mathrm{Tr}_c L^\dagger)/N_C$. The Polyakov loop L is a matrix in color space

$$L(\vec{x}) = \mathcal{P}\exp\left[i\int_0^\beta d\tau A_4(\vec{x},\tau)\right], \tag{2}$$

where $\beta = 1/T$ is the inverse of temperature and $A_4 = iA_0$.

In the mean field approximation, the constituent quark mass can be derived as

$$M_i = m_i - 4G\phi_i + 2K\phi_j\phi_k \quad (i \neq j \neq k), \tag{3}$$

where ϕ_i stands for quark condensate of the flavor i. The thermodynamical potential of bulk quark matter is derived as [55–60]

$$\begin{aligned}\Omega &= U(\bar{\Phi}, \Phi, T) + 2G({\phi_u}^2 + {\phi_d}^2 + {\phi_s}^2) - 4K\phi_u\phi_d\phi_s \\ &\quad - 2\int_\Lambda \frac{\mathrm{d}^3p}{(2\pi)^3} 3(E_u + E_d + E_s) \\ &\quad - 2T\sum_{i=u,d,s}\int \frac{\mathrm{d}^3p}{(2\pi)^3}(\ln\mathcal{A}_1 + \ln\mathcal{A}_2), \end{aligned} \tag{4}$$

where $\mathcal{A}_1 = 1 + 3\Phi e^{-(E_i-\mu_i)/T} + 3\bar{\Phi}e^{-2(E_i-\mu_i)/T} + e^{-3(E_i-\mu_i)/T}$, $\mathcal{A}_2 = 1 + 3\bar{\Phi}e^{-(E_i+\mu_i)/T} + 3\Phi e^{-2(E_i+\mu_i)/T} + e^{-3(E_i+\mu_i)/T}$, and μ_i is the quark chemical potential. $E_i = \sqrt{\mathbf{p}^2 + M_i^2}$ is the dispersion relation of quark in isotropic QCD medium.

The Polyakov-loop effective potential [59] taken in this study is

$$\begin{aligned}\frac{U(\Phi,\bar{\Phi},T)}{T^4} &= -\frac{a(T)}{2}\bar{\Phi}\Phi + b(T)\ln[1 - 6\bar{\Phi}\Phi \\ &\quad + 4(\bar{\Phi}^3 + \Phi^3) - 3(\bar{\Phi}\Phi)^2], \end{aligned} \tag{5}$$

where

$$a(T) = a_0 + a_1\left(\frac{T_0}{T}\right) + a_2\left(\frac{T_0}{T}\right)^2 \ \ \mathtt{and} \ \ b(T) = b_3\left(\frac{T_0}{T}\right)^3. \tag{6}$$

The logarithmic effective potential in Eq. (5) effectively includes the Vandermonde term from the Jacobian of transformation from Wilson line to Polyakov loop, and it rectifies the anomaly of traced Polyakov loop with $\Phi > 1$ at high temperature for a simple polynomial form of $U(\Phi, \bar{\Phi}, T)$ [10].

The parameters a_i, b_i listed in Table I are fitted according to the lattice simulation of QCD thermodynamics in pure gauge sector, and $T_0 = 210$ MeV is implemented in the calculation. In the numerical calculation, a cutoff Λ is implemented in three-momentum space for divergent integrations. We take the model parameters obtained in [61]: $\Lambda = 602.3$ MeV, $G\Lambda^2 = 1.835$, $K\Lambda^5 = 12.36$, $m_{u,d} = 5.5$, and $m_s = 140.7$ MeV, determined by fitting $f_\pi = 92.4$ MeV, $M_\pi = 135.0$ MeV, $m_K = 497.7$ MeV, and $m_\eta = 957.8$ MeV.

TABLE I. Parameters in the Polyakov-loop potential [59].

a_0	a_1	a_2	b_3
3.51	−2.47	15.2	−1.75

By minimizing the thermodynamical potential,

$$\frac{\partial\Omega}{\partial\phi_u}=\frac{\partial\Omega}{\partial\phi_d}=\frac{\partial\Omega}{\partial\phi_s}=\frac{\partial\Omega}{\partial\Phi}=\frac{\partial\Omega}{\partial\bar{\Phi}}=0, \tag{7}$$

we can derive the equations of motion in medium as

$$\phi_i=-2N_c\int\frac{d^3p}{(2\pi)^3}\frac{M_i}{E_i}(1-f_i(p)-\bar{f}_i(p)) \quad (i=u,d,s), \tag{8}$$

$$\frac{\partial U}{\partial\Phi}-6T\sum_{i=uds}\int\frac{d^3p}{(2\pi)^3}\left(\frac{1}{\mathcal{A}_1}e^{-\frac{E_i-\mu_i}{T}}+\frac{1}{\mathcal{A}_2}e^{-2\frac{E_i+\mu_i}{T}}\right)=0, \tag{9}$$

and

$$\frac{\partial U}{\partial\bar{\Phi}}-6T\sum_{i=uds}\int\frac{d^3p}{(2\pi)^3}\left(\frac{1}{\mathcal{A}_1}e^{-2\frac{E_i-\mu_i}{T}}+\frac{1}{\mathcal{A}_2}e^{-\frac{E_i+\mu_i}{T}}\right)=0. \tag{10}$$

In Eq. (8),

$$f_i(p)=\frac{\Phi e^{-(E_i-\mu_i)/T}+2\bar{\Phi}e^{-2(E_i-\mu_i)/T}+e^{-3(E_i-\mu_i)/T}}{1+3\Phi e^{-(E_i-\mu_i)/T}+3\bar{\Phi}e^{-2(E_i-\mu_i)/T}+e^{-3(E_i-\mu_i)/T}} \tag{11}$$

and

$$\bar{f}_i(p)=\frac{\bar{\Phi}e^{-(E_i+\mu_i)/T}+2\Phi e^{-2(E_i+\mu_i)/T}+e^{-3(E_i+\mu_i)/T}}{1+3\bar{\Phi}e^{-(E_i+\mu_i)/T}+3\Phi e^{-2(E_i+\mu_i)/T}+e^{-3(E_i+\mu_i)/T}} \tag{12}$$

are modified Fermion distribution functions of quark and antiquark, respectively. For a given temperature and chemical potential, the values of order parameters, ϕ_u, ϕ_d, ϕ_s, Φ, and $\bar{\Phi}$ can be derived by solving Eqs. (8)–(10).

For anisotropic quark matter, the dispersion relation of quasiparticles needs to be modified according to the anisotropic momentum distribution. In this study we take the Romatschke and Strickland scheme [44] in which the nontrivial dispersion relation for a particle with mass m is described by

$$E^{\text{aniso}}=\sqrt{\mathbf{p}^2+\xi(\mathbf{p}\cdot\mathbf{n})^2+m^2}. \tag{13}$$

Correspondingly, the distribution function of bosons and fermions at temperature T and chemical potential μ is

$$f^{\text{aniso}}(\mathbf{p})=\frac{1}{[\exp(\sqrt{\mathbf{p}^2+\xi(\mathbf{p}\cdot\mathbf{n})^2+m^2}-\mu)/T]\pm1}, \tag{14}$$

where $\mathbf{n}$ is the unit vector along the anisotropy direction. The anisotropic parameter ξ is defined as

$$\xi=\frac{\langle p_\perp^2\rangle}{2\langle p_\parallel^2\rangle}-1, \tag{15}$$

where $p_\parallel=\mathbf{p}\cdot\mathbf{n}$ is the momentum component parallel to the direction $\mathbf{n}$, and $p_\perp=|\mathbf{p}-(\mathbf{p}\cdot\mathbf{n})\cdot\mathbf{n}|$ is the component perpendicular to $\mathbf{n}$. The range of ξ is $-1<0<\infty$, which indicates the strength and type of momentum-space anisotropy. The momentum distribution is isotropic for $\xi=0$. For $\xi>0$, the momentum distribution is squeezed along $\mathbf{n}$ direction. For $-1<\xi<0$, it corresponds to a stretched momentum distribution along the direction $\mathbf{n}$.

Such a parametrization is interesting in heavy-ion collisions with the momentum distribution to be squeezed or stretched along one direction. Combined with the heavy-ion collision experiments, it is reasonable and convenient to choose $\mathbf{n}$ along the direction of nucleon-nucleon collision. With this parametrization the dispersion relation for quarks and antiquarks becomes

$$E_i^{\text{aniso}}=\sqrt{p^2+\xi p^2\cos\theta^2+M_i^2}. \tag{16}$$

The dispersion relation $E_i=\sqrt{\mathbf{p}^2+M_i^2}$ in isotropic matter in Eqs. (3)–(12) will be replaced with the new one to explore the properties of anisotropic quark matter. At the same time, all the relevant three-dimensional integrations will be performed with the consideration of anisotropic momentum distribution. We assume that the gluon field is a background field, so the anisotropic distribution of quark momentum does not affect the form of $U(\Phi,\bar{\Phi},T)$. The modeling of anisotropic medium primarily relies on a quasiparticle description where the medium effects are encoded in the effective distribution functions.

III. NUMERICAL RESULTS AND DISCUSSIONS

To understand the anisotropic distribution of momentum under different parameter ξ with a dynamical quark mass, we first plot in Fig. 1 the angular dependence of the average momentum of $u(d)$ quark for $\xi=-0.4, 0, 0.4$, respectively. The mean value of momentum at the angle θ is defined as

$$\bar{p}(\theta,\xi)=\frac{\int_0^\infty pf(p,\theta,\xi)dp}{\int_0^\infty f(p,\theta,\xi)dp}, \tag{17}$$

where the quark distribution function $f(p,\theta,\xi)$ is given in Eq. (11) with the modified dispersion relation in Eq. (16). The function $f(p,\theta,\xi)$ also depends on the order parameters $(\phi_i,\Phi,\bar{\Phi})$, which are determined for a given T and μ_B by solving Eqs. (8)–(10). As an example, the average of angular dependent momentum shown in Fig. 1 is calculated at $T=180$ MeV and $\mu_B=0$.

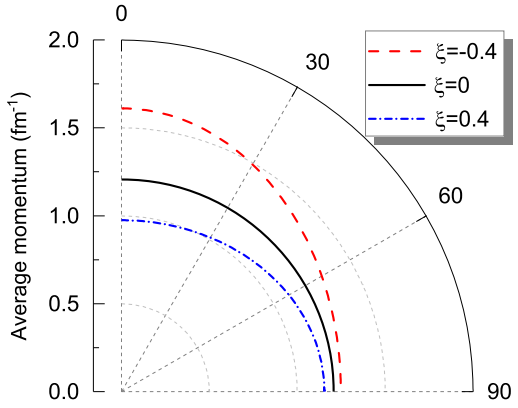

FIG. 1. Angular dependence of average momentum of $u(d)$ quark for $\xi = -0.4,\ 0,\ 0.4$ at $T = 180$ MeV and $\mu_B = 0$. Assuming $\theta = 0$ is the anisotropic direction n.

In the case of $\xi = 0$, Fig. 1 shows that $\bar{p}(\theta, \xi)$ is independent of angle θ, which is just the feature of momentum isotropy. In the case of $\xi = -0.4$, the average of momentum is anisotropic with a maximum value at $\theta = 0$ (i.e., along the anisotropic direction n) and a minimum value at 90°, perpendicular to the anisotropic direction n. The opposite happens in the case of $\xi = 0.4$. With the assumption of $\theta = 0$ being the anisotropic direction n, Fig. 1 clearly demonstrates that the anisotropic momentum is stretched along the anisotropic direction n for $\xi < 0$ and squeezed for $\xi > 0$.

In Fig. 2, we further present the angular dependence of quark distribution function $f(p, \theta, \xi)$ for different ξ with several fixed momentums, $p = 0.5,\ 1,\ 1.5,\ 2$ fm^{-1}. This figure shows that $f(p, \theta, \xi)|_p$ descends (increases) as θ increases from 0° to 90° for $\xi = -0.4$ ($\xi = 0.4$). It also indicates that, at a fixed angle, the anisotropy of $f(p, \theta, \xi)$ changes for different ξ at the same momentum p. This possibly provides a potential method to test the anisotropic

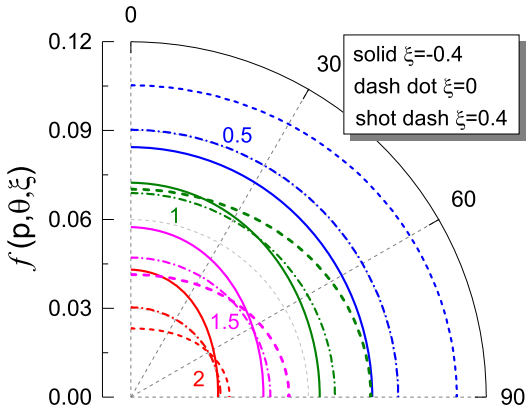

FIG. 2. Angular dependence of quark distribution function $f(p, \theta, \xi)$ for $\xi = -0.4,\ 0,\ 0.4$ with several fixed momentums, $p = 0.5,\ 1,\ 1.5,\ 2$ fm^{-1} at $T = 180$ MeV and $\mu_B = 0$. $\theta = 0$ is the anisotropic direction.

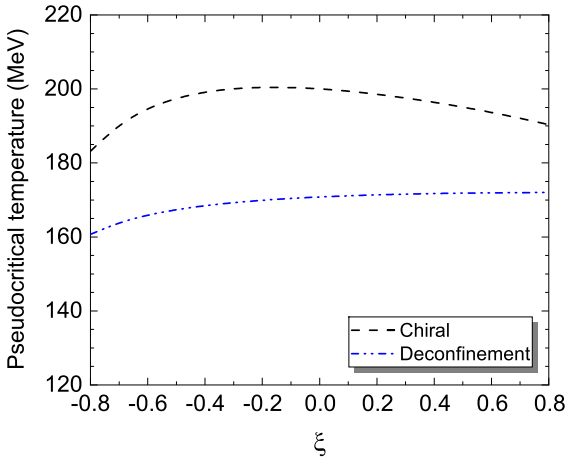

FIG. 3. Pseudocritical critical temperatures of the chiral and (de)confinement transformation as functions of anisotropic parameter ξ.

parameter ξ if the angular and momentum dependence of particle distribution in HIC experiments is available. A further study will be carried on this issue.

Now we investigate the QCD phase transition at vanishing chemical potential with different anisotropic parameter ξ. We plot in Fig. 3 the pseudocritical critical temperatures of both the chiral and deconfinement transformation derived at $\mu_B = 0$ as functions of anisotropic parameter ξ. For each value of ξ, the pseudocritical temperature of chiral phase transition (T_χ) is derived at the location where $(\partial\phi_u/\partial T)_{\mu_B=0}$ takes the maximum. Similarly, the pseudocritical temperature of deconfinement transformation (T_D) is derived with the condition of $(\partial\Phi/\partial T)_{\mu_B} = 0$ taking the maximum. Figure 3 shows that the pseudocritical temperature of color deconfinement increases monotonically with the increase of ξ. However, the pseudocritical temperature of chiral crossover changes nonmonotonically with the variation of ξ. The maximum value of T_χ appear at $\xi = -0.16$. Note also that $T_\chi(\xi)$ is not simply symmetrical on both sides of $\xi = 0$.

Note that in this version of PNJL model the locations of chiral and deconfinement transitions do not coincide at vanishing chemical potential. Some extensions, such as considering the entanglement interaction between the chiral condensate and the Polyakov loop or the eight-quark interaction, can reduce the difference between them to some extent. In this study we temporarily ignore these factor, and focus on the different effect of anisotropic momentum distribution on the pseudocritical temperatures of the two phase transitions with different ξ in this model.

The full QCD phase diagrams are plotted in Fig. 4(b) for the isotropic quark matter ($\xi = 0$) and in Fig. 4(a) and (c) for the anisotropic quark matter with $\xi = \pm 0.4$. Figure 4 indicates that there is a close relationship between the phase structure and the anisotropic parameter ξ, in particular, in the area near the critical region and the first-order phase

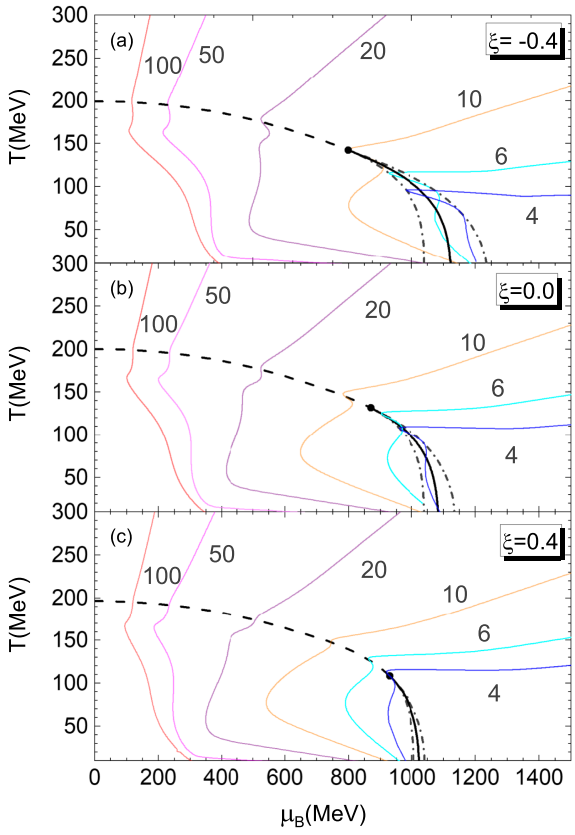

FIG. 4. QCD phase diagrams for different anisotropic parameter. (a) $\xi = -0.4$ with a stretched momentum distribution along the anisotropic direction, (b) $\xi = 0$ with a isotropic momentum distribution, (c) $\xi = 0.4$ with a squeezed momentum distribution along the anisotropic direction. The isentropic trajectories with $s/\rho_B = 100, 50, 20, 10, 6, 4$ are also plotted in the three cases.

transition. In the case of $\xi = -0.4$ with a stretched momentum distribution along the anisotropic direction, the CEP of chiral phase transition moves to a higher temperature and smaller chemical potential, compared with the isotropic quark matter with $\xi = 0$. The associated spinodal region of the first-order phase transition is correspondingly enlarged, which means that the metastable and unstable phases exist in more wider range. Figure 4(a) also shows that at lower temperatures the first-order phase transition has a larger chemical potential than that of $\xi = 0$. Compared with the result of $\xi = -0.4$, in the case of $\xi = 0.4$ with a squeezed momentum distribution along the anisotropic direction, the opposite trend appears, and the range of first-order phase transition as well as the associated spinodal structure shrink in the phase diagram. Additionally, with the inclusion of entanglement interaction or eight-quark interaction, the numerical results indicate that the QCD phase structure shows a similar trend at low temperature as shown in Fig. 4.

The isentropic trajectories are also plotted in Fig. 4 for different anisotropic parameter ξ. It can be seen that the relation between the isentropic trajectories for $s/\rho_B < 20$ and the phase structure at high density highly depends on the type of anisotropy (stretched or squeezed in the momentum space). For example, the trajectory of $s/\rho_B = 6$ in the phase diagram with $\xi = 0.4$ in Fig. 4(c) passes through the chiral crossover transformation line, but the isentropic trajectory with the same s/ρ_B for $\xi = -0.4$ in Fig. 4(a) passes through the first-order phase transition. Since the entropy per baryon is connected to the collision energy in HIC experiments, the estimate of the initial entropy density and entropy density per baryon can be extracted for different center-of-mass energies [62].

Because the fluctuations of conserved charges are sensitive to the QCD phase structure, they are naturally relevant to the anisotropy of momentum distribution in HIC experiments. We plot in Figs. 5 and 6 the net baryon number kurtosis and skewness as functions of temperature and chemical potential for different anisotropic parameter ξ. Combined with the phase diagram in Figs. 4, 5(a), and 6(a) show that, at higher temperatures closed to the chiral

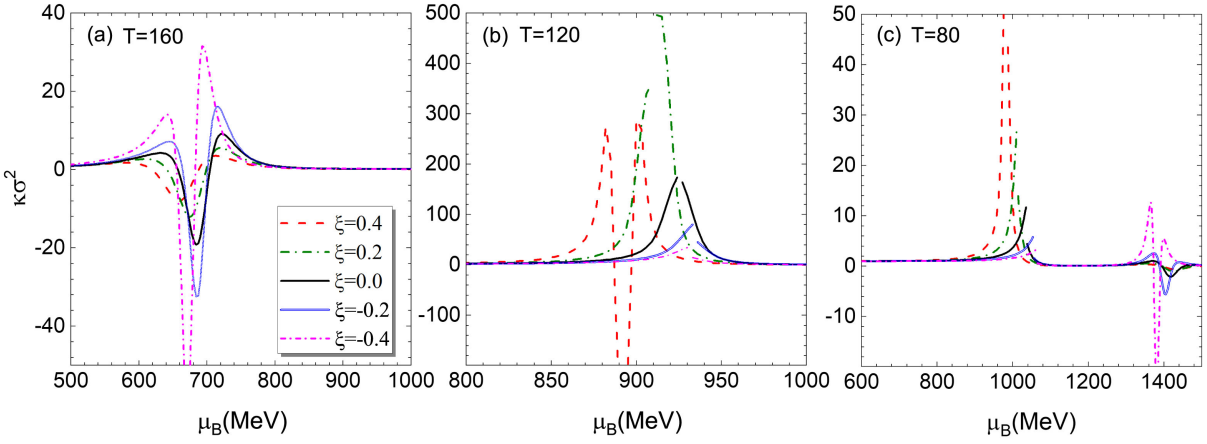

FIG. 5. Baryon number kurtosis (a) near the crossover phase transition, (b) near the critical region, (c) near the first-order region.

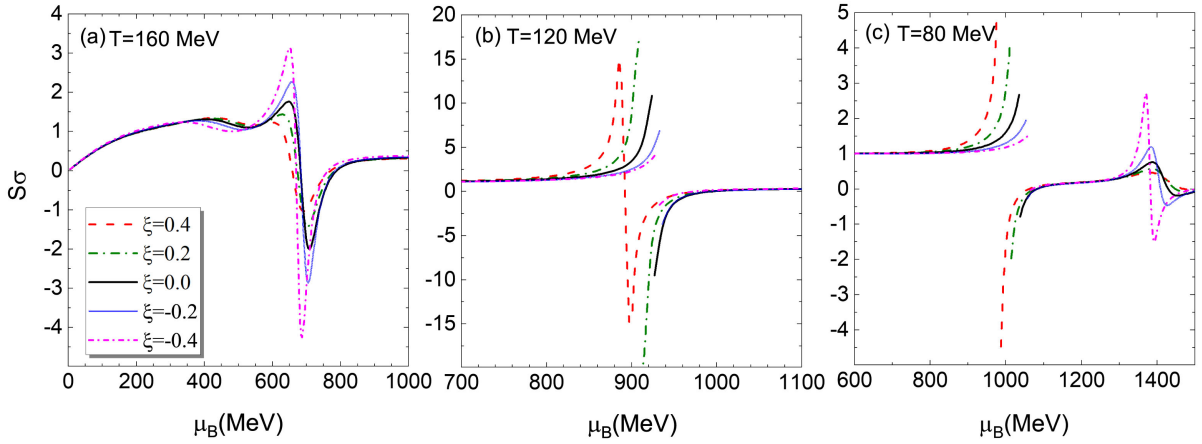

FIG. 6. Baryon number skewness (a) near the crossover phase transition, (b) near the critical region, (c) near the first-order region.

crossover, the kurtosis and skewness in the case of $\xi = -0.4$ with a stretched momentum distribution along the anisotropic direction are stronger than the squeezed ($\xi = 0.4$) and isotropic ($\xi = 0$) ones. However, Figs. 5(b) and 6(b) indicate that with the decrease of temperature the values of kurtosis and skewness for $\xi = 0.4$ are larger than those for isotropic ($\xi = 0$) and stretched momentum distribution ($\xi < 0$) at temperatures near the critical region. Figures 5(c) and 6(c) also indicate the similar result in the first-order phase transition region. The fluctuations at larger chemical potentials are induced by the chiral phase transition of strange quark. According to the hydrodynamic simulations and HIC experiments, the squeezed momentum distribution along the beam direction ($\xi > 0$) is supported. Therefore, compared with the isotropic quark matter, the values of net baryon kurtosis and skewness are possibly enhanced in anisotropic medium with the decrease of collision energies. The exact results depend on how far the chemical freeze-out line is away from the phase transition line as well as the anisotropic parameter ξ.

The comparative study of net baryon number fluctuations in low-energy effective models, lattice QCD, and heavy-ion collision experiments are important in predicting the QCD phase structure at high density. However, when the anisotropic momentum distribution is considered, the accomplishment of this task is beyond reach at present due to the lack of research in lattice QCD and experimental data. Besides, the relationship between collision centrality, colliding energy, and the anisotropic parameter ξ are still unknown. The release of more BES II data in the future may provide an opportunity to investigate these aspects. When conditions permit, a comparison of the kurtosis and skewness of net baryon number fluctuations with the anisotropy of quark momentum in this effective model with those of experimental data and/or lattice QCD will be conducted. Only some qualitative results are presented in this preliminary investigation.

IV. SUMMARY

In this work, we studied the properties of quark matter with the anisotropic momentum distribution in the PNJL model. We analyzed the features of angular dependence of average momentum and quark distribution function for different types of momentum anisotropy in the Romatschke and Strickland scheme. The numerical results indicate that the squeezed (stretched) momentum distribution along the anisotropic direction can be effectively described with the anisotropic parameter $\xi > 0$ ($\xi < 0$). The calculation also suggests that the QCD phase structure are closely related to the anisotropic parameter ξ, in particular in the high density region. In the case of stretched momentum distribution with $\xi < 0$, the range of first-order phase transition are enlarged and the CEP moves to a lower temperature and smaller chemical potential. The opposite situation occurs in the case of squeezed momentum distribution with $\xi > 0$.

We further calculated the kurtosis and skewness of net baryon number fluctuations for different anisotropic parameter. Since the squeezed momentum distribution along the beam direction is supported by experimental data and hydrodynamic simulations, $\xi > 0$ is required to describe the HIC experiments. In this case, the numerical results show that the kurtosis and skewness of net baryon number distribution at lower collision energies are possibly larger than those of isotropic quark matter. The accuracy depends on the locations of QCD phase transition and the chemical freeze-out line as well as the real anisotropic parameter ξ in experiments. A comparative study of fluctuations and correlations of conserved charges in quark models with experimental data and lattice QCD will be performed when conditions permit in the future.

ACKNOWLEDGMENTS

This work is supported by the National Natural Science Foundation of China under Grant No. 11875213.

[1] Y. Aoki, G. Endrodi, Z. Fodor, S. D. Katz, and K. K. Szabo, Nature (London) **443**, 675 (2006).
[2] S. Gupta, X. F. Luo, B. Mohanty, H. G. Ritter, and N. Xu, Science **332**, 1525 (2011).
[3] A. Bazavov, T. Bhattacharya, M. Cheng, C. DeTar, H. T. Ding, S. Gottlieb *et al.* (hotQCD Collaboration), Phys. Rev. D **85**, 054503 (2012).
[4] S. Borsányi, Z. Fodor, S. D. Katz, S. Krieg, C. Ratti, and K. K. Szabó, Phys. Rev. Lett. **111**, 062005 (2013).
[5] A. Bazavov, T. Bhattacharya, C. DeTar, H. T. Ding, S. Gottlieb, R. Gupta *et al.*, Phys. Rev. D **90**, 094503 (2014).
[6] A. Bazavov, H. T. Ding, P. Hegde, O. Kaczmarek, F. Karsch, E. Laermann *et al.* (hotQCD Collaboration), Phys. Rev. D **96**, 074510 (2017).
[7] S. Borsányi, Z. Fodor, C. Hoelbling, S. D. Katz, S. Krieg, and K. K. Sabzó, Phys. Lett. B **730**, 99 (2014).
[8] S. Borsányi, Z. Fodor, J. N. Guenther, R. Kara, S. D. Katz, P. Parotto, A. Pasztor, C. Ratti, and K. K. Szabo, Phys. Rev. Lett. **125**, 052001 (2020).
[9] K. Fukushima, Phys. Rev. D **77**, 114028 (2008).
[10] C. Ratti, M. A. Thaler, and W. Weise, Phys. Rev. D **73**, 014019 (2006).
[11] P. N. Meisinger and M. C. Ogilvie, Phys. Lett. B **379**, 163 (1996).
[12] P. Costa, M. C. Ruivo, C. A. de Sousa, and H. Hansen, Symmetry **2**, 1338 (2010).
[13] T. Sasaki, J. Takahashi, Y. Sakai, H. Kouno, and M. Yahiro, Phys. Rev. D **85**, 056009 (2012).
[14] M. Ferreira, P. Costa, and C. Providência, Phys. Rev. D **89**, 036006 (2014).
[15] B. J. Schaefer, M. Wagner, and J. Wambach, Phys. Rev. D **81**, 074013 (2010).
[16] V. Skokov, B. Friman, and K. Redlich, Phys. Rev. C **83**, 054904 (2011).
[17] S. X. Qin, L. Chang, H. Chen, Y. X. Liu, and C. D. Roberts, Phys. Rev. Lett. **106**, 172301 (2011).
[18] F. Gao, J. Chen, Y. X. Liu, S. X. Qin, C. D. Roberts, and S. M. Schmidt, Phys. Rev. D **93**, 094019 (2016).
[19] C. S. Fischer, J. Luecker, and C. A. Welzbacher, Phys. Rev. D **90**, 034022 (2014).
[20] K. Maslov and D. Blaschke, Phys. Rev. D **107**, 094010 (2023).
[21] W. J. Fu, J. M. Pawlowski, and F. Rennecke, Phys. Rev. D **101**, 054032 (2020).
[22] G. Y. Shao, Z. D. Tang, X. Y. Gao, and W. B. He, Eur. Phys. J. C **78**, 138 (2018).
[23] L. M. Liu, J. Xu, and G. X. Peng, Phys. Rev. D **104**, 076009 (2021).
[24] M. A. Stephanov, Phys. Rev. Lett. **102**, 032301 (2009); **107**, 052301 (2011).
[25] X. Luo and N. Xu, Nucl. Sci. Tech. **28**, 112 (2017).
[26] J. Adam, L. Adamczyk, J. R. Adams, J. K. Adkins, G. Agakishiev, and M. M. Aggarwal, Phys. Rev. Lett. **126**, 092301 (2021).
[27] B. E. Aboona, J. Adam, L. Adamczyk, J. R. Adams, I. Aggarwal, M. M. Aggarwal *et al.* (The STAR Collaboration), Phys. Rev. Lett. **130**, 082301 (2023).
[28] A. Dumitru, Y. Guo, A. Mocsy, and M. Strickland, Phys. Rev. D **79**, 054019 (2009).
[29] P. Huovinen, P. Kolb, U. Heinz, P. Ruuskanen, and S. Voloshin, Phys. Lett. B **503**, 58 (2001).
[30] T. Hirano and K. Tsuda, Phys. Rev. C **66**, 054905 (2002).
[31] A. Muronga, Phys. Rev. Lett. **88**, 062302 (2002).
[32] U. W. Heinz, H. Song, and A. K. Chaudhuri, Phys. Rev. C **73**, 034904 (2006).
[33] P. Romatschke and U. Romatschke, Phys. Rev. Lett. **99**, 172301 (2007).
[34] H. Song and U. W. Heinz, Phys. Lett. B **658**, 279 (2008).
[35] G. S. Denicol, T. Koide, and D. H. Rischke, Phys. Rev. Lett. **105**, 162501 (2010).
[36] E. Calzetta, Phys. Rev. D **92**, 045035 (2015).
[37] G. S. Denicol, S. Jeon, and C. Gale, Phys. Rev. C **90**, 024912 (2014).
[38] A. Jaiswal, R. Ryblewski, and M. Strickland, Phys. Rev. C **90**, 044908 (2014).
[39] L. Tinti and W. Florkowski, Phys. Rev. C **89**, 034907 (2014).
[40] M. Alqahtani, M. Nopoush, and M. Strickland, Prog. Part. Nucl. Phys. **101**, 204 (2018).
[41] M. Alqahtani, M. Nopoush, R. Ryblewski, and M. Strickland, Phys. Rev. Lett. **119**, 042301 (2017).
[42] D. Almaalol, M. Alqahtani, and M. Strickland, Phys. Rev. C **99**, 044902 (2019).
[43] H. Alalawi and M. Strickland, Phys. Rev. C **102**, 064904 (2020).
[44] P. Romatschke and M. Strickland, Phys. Rev. D **68**, 036004 (2003).
[45] M. E. Carrington, B. M. Forster, and S. Makar, Phys. Rev. C **104**, 064908 (2021).
[46] A. Dumitru, Y. Guo, and M. Strickland, Phys. Rev. D **79**, 114003 (2009).
[47] K. Boguslavski, B. S. Kasmaei, and M. Strickland, J. High Energy Phys. 10 (2021) 083.
[48] S. Hauksson, S. Jeon, and C. Gale, Phys. Rev. C **103**, 064904 (2021).
[49] B. S. Kasmaei and M. Strickland, Phys. Rev. D **102**, 014037 (2020).
[50] L. Thakur, P. K. Srivastava, G. P. Kadam, M. George, and H. Mishra, Phys. Rev. D **96**, 096009 (2017).
[51] S. Rath and B. K. Patra, Phys. Rev. D **100**, 016009 (2019).
[52] G. Y. Shao, X. Y. Gao, and W. B. He, Phys. Rev. D **101**, 074029 (2020).
[53] W. J. Fu, X. F. Luo, J. M. Pawlowski, F. Rennecke, R. Wen, and S. Yin, Phys. Rev. D **104**, 094047 (2021).
[54] W. B. He, G. Y. Shao, X. Y. Gao, X. R. Yang, and C. L. Xie, Phys. Rev. D **105**, 094024 (2022).
[55] K. Fukushima, Phys. Lett. B **591**, 277 (2004).
[56] P. N. Meisinger and M. C. Ogilvie, Nucl. Phys. B, Proc. Suppl. **47**, 519 (1996).
[57] S. K. Ghosh, T. K. Mukherjee, M. G. Mustafa, and R. Ray, Phys. Rev. D **77**, 094024 (2008).
[58] S. Mukherjee, M. G. Mustafa, and R. Ray, Phys. Rev. D **75**, 094015 (2007).
[59] S. Rößner, C. Ratti, and W. Weise, Phys. Rev. D **75**, 034007 (2007).
[60] S. K. Ghosh, T. K. Mukherjee, M. G. Mustafa, and R. Ray, Phys. Rev. D **73**, 114007 (2006).
[61] P. Rehberg, S. P. Klevansky, and J. Hufner, Phys. Rev. C **53**, 410 (1996).
[62] M. Motta, R. Stiele, W. M. Alberico, and A. Beraudo, Eur. Phys. J. C **80**, 770 (2020).